phys. stat. sol. (a) **125**, 635 (1991)

Subject classification: 75.60 and 75.70; S1.1; S1.2

Institut für Werkstoffwissenschaften der Universität Erlangen-Nürnberg[1]) *(a) and Institut für Festkörperforschung, Kernforschungsanlage Jülich*[2]) *(b)*

Domain Observations on Fe–Cr–Fe Layered Structures

Evidence for a Biquadratic Coupling Effect

By

M. RÜHRIG (a), R. SCHÄFER (a), A. HUBERT (a), R. MOSLER (b), J. A. WOLF (b), S. DEMOKRITOV[3]) (b), and P. GRÜNBERG (b)

The recently discovered oscillating exchange effect in iron–chromium multilayers can best be studied on an epitaxial iron sandwich with a wedge shaped chromium interlayer. Domain patterns are analyzed as well as magnetization curves on such samples using magnetooptical techniques. Unusual domains are found in zones around the transitions between ferromagnetic and antiferromagnetic exchange. Also the magnetization curves for larger chromium thickness show some peculiar features. The interpretation of these patterns invokes coupling between the iron layers which favours a right angle between the magnetization directions in both layers. Such a non-collinear interaction can be derived phenomenologically from a biquadratic coupling as introduced earlier in the analysis of spin structures in oxides. A biquadratic coupling can be understood either as a second order Heisenberg or a second order Dzyaloshinskii interaction. In the course of these investigations domain observations proved to be a useful and sensitive method to detect locally the nature of interactions between ferromagnetic layers.

Die kürzlich entdeckte oszillierende Wechselwirkung in Eisen Chrom-Vielfachschichten kann am besten an einer epitaxialen Schichtanordnung mit einer keilförmigen Chromzwischenschicht studiert werden. Die auf solchen Proben beobachtbaren Domänenstrukturen sowie die Magnetisierungskurven werden mit magnetooptischen Verfahren untersucht. Im Bereich der Übergänge zwischen ferromagnetischer und antiferromagnetischer Kopplung werden Zonen ungewöhnlicher Muster entdeckt. Auch die Magnetisierungskurven für größere Chrom-Schichtdicken zeigten eigentümliche Züge. Die Beobachtungen lassen sich erklären, wenn eine zusätzliche Kopplung der Schichten angenommen wird, die einen rechten Winkel zwischen den Magnetisierungsrichtungen in beiden Schichten begünstigt. Phänomenologisch ergibt sich eine solche nicht-kollineare Kopplung aus der Annahme einer biquadratischen Wechselwirkung, wie sie früher in der Analyse von Spinstrukturen magnetischer Oxide eingeführt wurde. Eine biquadratische Kopplung läßt sich entweder als Heisenberg- oder Dzyaloshinskii-Wechselwirkung zweiter Ordnung interpretieren. Domänenbeobachtungen erwiesen sich im Laufe dieser Untersuchung als empfindliche Methode zur Untersuchung des Charakters der Kopplung in Vielfachschichten.

1. Introduction

A few years ago an antiferromagnetic interaction between iron films separated by thin chromium interlayers of a certain thickness range was identified by an analysis of the spin waves in these structures [1]. It was quite a surprise when this exchange interaction was later found to *oscillate* as a function of the chromium thickness. This discovery was achieved by recording and analyzing magnetization (and magnetoresistance) curves [2]. The period of the oscillation covers many lattice planes and is not commensurate with the lattice

[1]) Martensstr. 7, W-8520 Erlangen, FRG.
[2]) Postf. 1913, W-5170 Jülich, FRG.
[3]) On leave from P. L. Kapitsa Institute for Physical Problems, Moscow, USSR.

constant of the chromium. Hysteresis measurements allow to measure the strength of the interaction as long as it is antiferromagnetic. Increasing the sensitivity of the mentioned spin wave methods the oscillatory nature of the interaction could be confirmed and a ferromagnetic coupling between the antiferromagnetic regimes, that is, a change of sign in the coupling constant, could be explicitly confirmed [3]. Although the observed damped oscillation of the exchange interaction recalls the picture of the classical RKKY interaction, no final theoretical treatment of the phenomenon seems to be available [4 to 7].

Iron- chromium multilayers display another interesting feature, namely a large magnetoresistive effect [8 – 10, 2] which differs in nature from the conventional orientation-dependent effect. It relies on the spin-dependent scattering of electrons at the interfaces of the film system and can be enhanced in multiple film systems. The potential giant magnetoresistance effect stimulated application-related interest in these samples.

Both from fundamental interest and in view of these applications we studied the magnetic domain patterns as well as magnetization curves on the same epitaxial systems which had been formerly used to measure the exchange effect by means of light scattering from spin waves [3]. A rich variety of domain patterns was observed, the careful analysis of which led to surprising insights and to the discovery of a new, unexpected kind of interaction. The same kind of interaction was derived from the observation of characteristic steps at half-saturation in the magnetization curves.

2. Experimental

The layer system was deposited by molecular beam epitaxy on a (100)-GaAs substrate of $6 \times 16\ mm^2$ dimension, a 1 nm iron seed layer, and a 150 nm silver buffer layer. (In the case of the first sample in Fig. 3 the seed layer was still 10 nm thick, which produced slightly less perfect growth which will also manifest itself in the domain observations.)

The technique produced very clear (100)-oriented single crystal iron films with no apparent crystal defects. LEED spot profiles, if evaluated qualitatively, indicate terrace widths of the order of 10 nm. The domain observations were mainly performed on systems consisting of two equal iron layers of 5 to 20 nm thickness each, separated by a slightly inclined wedge of chromium, varying over a length of 16 mm from zero to 2 to 10 nm thickness. The whole system is covered and protected by a ZnS antireflection coating which enhances at the same time the magnetooptical effects. With this protection the sample can be handled in air without apparent deterioration. The anisotropy of the films agrees with that of the bulk material, with the easy directions along the $\langle 100 \rangle$ axes. Domains on samples with larger iron layer thickness and on a polycrystalline sample were also observed (this sample was deposited on a glass substrate in the same apparatus and under similar conditions as in the MBE experiments).

Easy axis magnetization curves were measured magnetooptically on samples with a larger interval of Cr and smaller Fe thickness in order to increase the effect of exchange interactions relative to coercivity effects, which amounted in all samples to values less than 5 Oe[4]).

The domains were observed magnetooptically in reflection using a digital contrast enhancement scheme [11]. In addition to the Kerr effect we employed the linear magnetic

[4]) The two lines of experiments reported in this paper, domain observation and the measurement of magnetization curves, had been performed independently. As they led to the same conclusions, they are published here together. Unfortunately, it was no more possible to observe the domain patterns on the same samples on which the magnetization curves had been measured.

birefringence (the Voigt effect) and the recently discovered magnetooptic gradient effect [12] in order to analyse complicated patterns. Starting with an overview based on a stereo microscope we used various magnifications up to oil immersion using an objective of 1.25 numerical aperture. Both a mercury arc lamp selecting the green and yellow spectrum lines and an argon laser illumination system were employed. Due to the opaque GaAs substrate, only the top side of the multilayer system could be investigated. The magnetooptical contrast thus is mainly determined by the top iron layer, but the bottom layer contributes for thin, transparent iron layers to some extent to the contrast. We observed this effect for iron thickness of 5 and 10 nm thickness, but no more for 20 nm or thicker films. In-plane fields could be applied during domain observation along all directions. They were large enough to saturate the sample along the relatively hard ⟨110⟩ directions.

It proved to be impossible to apply the quantitative Kerr technique [13] which compares domain intensities with saturation intensities to the sandwich samples with transparent iron films, except for the (trivial) case of ferromagnetic coupling. The problem arises when the magnetization directions in the two layers are not aligned at low fields but aligned at high fields. The grey shades at low fields are then not related to the contrasts at saturation. For this reason carefully adjusted combination experiments [12] in which the same domain pattern is recorded in different magnetooptical aspects were primarily used to unravel the observations.

3. Results and Discussion

3.1 Domains: overview

Fig. 1 shows an overview of the domains on the thin-chromium side of a (Fe 10 nm | Cr 0 to 3.7 nm | Fe 10 nm) sample. Visible are a first, easily magnetizable ferromagnetically coupled area for which the chromium layer is thinner than 0.5 nm, and a wider area with a much higher saturation field which according to other evidence is coupled antiferromagnetically. The ferromagnetic section is characterized by domain patterns with four phases magnetized along the four easy directions. The regular features of the domains in the ferromagnetic region become visible at higher resolution. The pattern in the antiferromagnetically coupled area does not represent any kind of an equilibrium pattern. Many different patterns can be generated depending on the history of the applied field, and again high resolution observations will shed more light on the behaviour of the domains in the antiferromagnetic regime.

Two interesting features are visible on the overview picture: The first observation is that domain walls inside the antiferromagnetic area can be generated which run perpendicular to the chromium thickness gradient, and which can be shifted smoothly in a sufficiently high applied field. To explain this observation one has to assume that the character and the strength of the effective coupling is a function of a continuous *mean* chromium layer thickness, averaged over a characteristic length of ferromagnetism in the two layers, and not by the local and necessarily discrete number of chromium lattice planes. The chromium layer must be rough within the exchange length to make this concept meaningful.

The second feature applies to the transition between the ferromagnetic and the antiferromagnetic areas. A narrow intermediate zone is visible there in which the character of the domain patterns differs markedly from the neighbouring patterns. Based on the slope of the chromium wedge the width of the intermediate zone can be evaluated. It corresponds

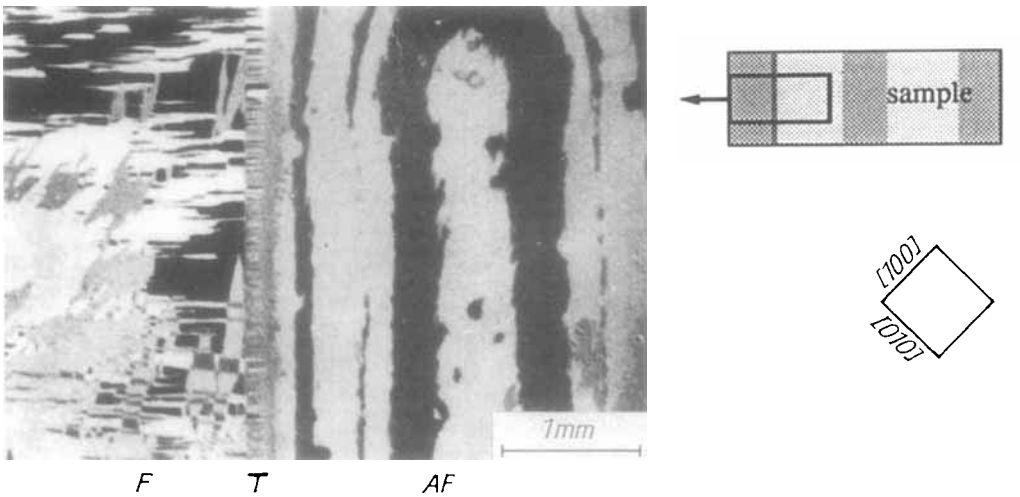

Fig. 1. Overview of the domain patterns of the part of a (Fe 10 nm | Cr 0 to 3.7 nm | Fe 10 nm) sample which is occupied by the first ferromagnetic and the first antiferromagnetic coupling area. The chromium layer thickness increases from zero on the left edge to about 1.1 nm on the right edge of the picture. Throughout the paper the letters F for a region of ferromagnetic coupling, AF for antiferromagnetic coupling, and T for the transition zone are used in the figures

to a chromium thickness interval of about 0.035 nm in this sample. Its sharp definition again confirms that only the averaged chromium thickness can be relevant.

A systematic scan of the magnetooptically measured switching field over the whole length of the sample, together with higher resolution domain views is shown in Fig. 2. The associated domain pictures were taken at remanence after saturating the sample along the hard direction transverse to the strip length.

The areas of low switching field are characterized by relatively wide domain patterns with domain walls oriented parallel and 45° to the easy directions. Such patterns are expected for (100)-oriented iron films and are a consequence of crystalline anisotropy and of the principle of flux-closure and stray field avoidance. Naturally we identify these segments with areas of ferromagnetic coupling between the two layers. This assigment is consistent with information available from spin wave measurements.

The segments of enhanced switching field are characterized by irregularly shaped domains. They can be understood assuming that in these parts of the sample the antiferromagnetic coupling prevails. If both layers are magnetized opposite to each other at every point in this area, their magnetic flux will cancel locally. Therefore, every orientation of a domain wall is possible, and the actual formation of walls will be determined by random influences. (Due to the very small chromium layer thickness residual stray fields between the two layers at the edges of domains have a very short range and are energetically negligible.)

Altogether three ferromagnetically and two antiferromagnetically coupled segments are observed on this sample. A domain pattern from one of the already mentioned transition zones between the ferromagnetic and antiferromagnetic segments is also shown in Fig. 2. More on this will follow in Section 3.3. Another, less pronounced transition was found in this sample between the first antiferromagnetic and the second ferromagnetic zone.

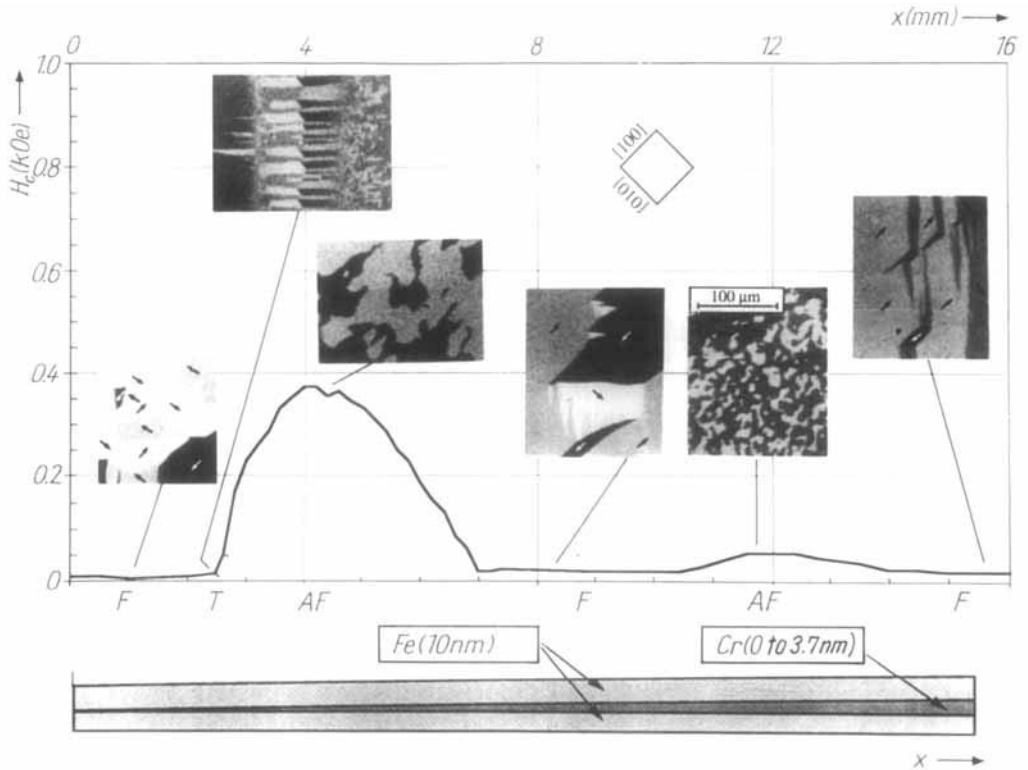

Fig. 2. Switching field and domain patterns along the whole length of the same sample as in Fig. 1. The switching field, also identified with the coercivity field, was determined by observing the domain pattern and registering its switching (complete reorganization) in the course of a hysteresis loop

The same studies were performed on a number of further samples in which the iron thickness varied between 5 and 20 nm. The results are collected schematically in Fig. 3. Basically the same features as presented before were found in all these samples. This can be pronounced if the data are plotted with the first transition between ferromagnetic and antiferromagnetic behaviour aligned. A problem is that the position of zero thickness (which is evaporated last) is not known accurately due to experimental conditions. Assuming that the well established first zero of the oscillating exchange interaction marks the same chromium thickness in all samples we obtain Fig. 3.

Comparing the different samples we observe the following:

1. The width of the first transition zone is in the majority of the samples close to an interval of 0.025 nm of Cr.

2. Except for the first sample in which higher transition zones were difficult to identify, all other samples showed well defined wide second and even third transition zones which increase in width to some extent with increasing order.

3. Beyond a chromium thickness of 2.5 nm domain observations do not allow a clear assignment of the nature of the exchange interaction at first sight.

4. Although the general features are similar in all samples, the details differ to some extent. This is most apparent for the width of the second and third transition zones relative to the width of the first one which vary rather strongly between the samples.

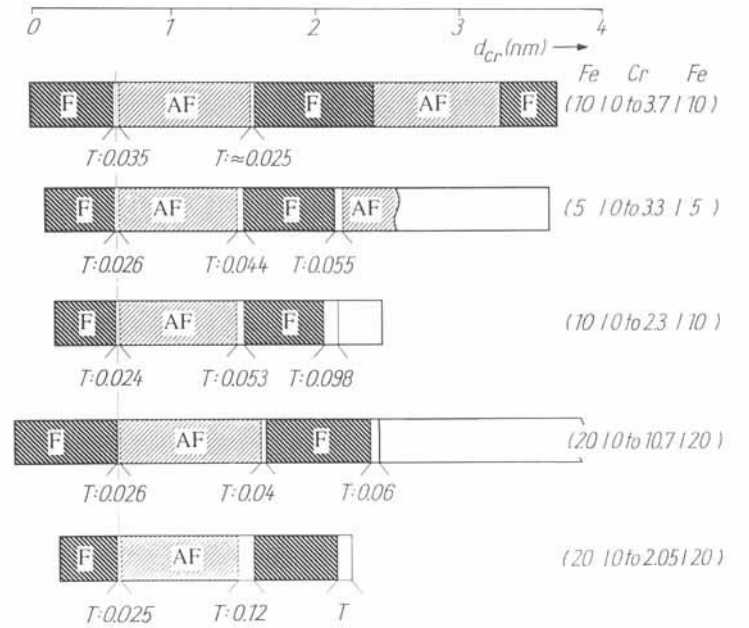

Fig. 3. A schematic representation of the observed domain types in five different samples. F stands for a zone with clearly ferromagnetically coupled layers, AF for antiferromagnetic coupling, and T for the transition zones demonstrated in Fig. 1 and 2. Unmarked zones display domains with weak, uncertain coupling. All thicknesses are given in nm

The differences between the samples cannot be attributed to obvious structural differences. The first sample did exhibit a less reversible domain behaviour in the ferromagnetic parts and in the transition zone. This sample, as mentioned in Section 2, was evaporated on a thicker iron seed layer and was known from LEED images to be less perfect structurally compared to the later systems. This may also explain the difficulties in identifying the second and higher transition zones. No obvious difference in the domain behaviour was observed between the four other samples.

In summary, transition zones with specific domain patterns differing clearly from the ferromagnetic and the antiferromagnetic zones were discovered in all investigated samples near the zeros of the oscillating exchange interaction. In the following sections their nature will be investigated in a systematic manner.

3.2 Domain nucleation

A particularly instructive feature will be discussed here which is observed when an applied field is reduced from the saturation field along an in-plane hard ⟨110⟩-direction. For this experiment the field must be adjusted precisely so that the rotation of the magnetization away from the hard direction is equally probable to either side. Under this condition two fundamentally different patterns are observed in ferromagnetically and in antiferromagnetically coupled zones (Fig. 4).

In the first case a conventional ripple pattern is formed (Fig. 4a), oriented transverse to the applied field due to magnetostatic effects [14 to 16]. In the other case of an

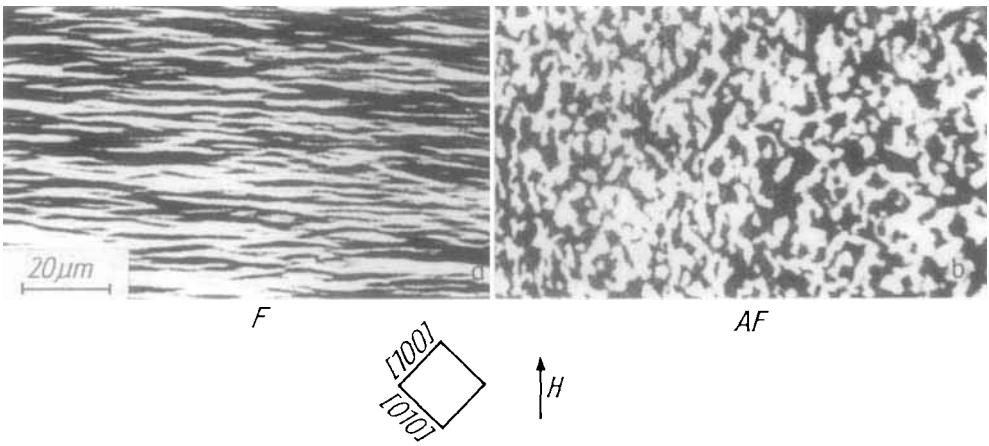

Fig. 4. a) "Ripple" and b) patch patterns observed on the (Fe 10 nm | Cr 0 to 3.7 nm | Fe 10 nm) sample after reducing an applied field from saturation along a hard direction. The strongly split domain pattern in a) develops out of a small-amplitude ripple pattern observable at nucleation

antiferromagnetic coupling an irregular patch pattern is seen (Fig. 4b). Here the transverse magnetization of the two layers can cancel and there is no reason for the formation of a ripple pattern. Fig. 5 indicates the difference between the ripple and the patch pattern in a schematic way.

The common origin of both the ripple and the patch pattern must be some random perturbation on a submicroscopic level. The atomic roughness of the chromium interlayer forms a natural source of random interactions in so far as it is not averaged out by lateral exchange stiffness. No explicit confirmation of this conjecture is available.

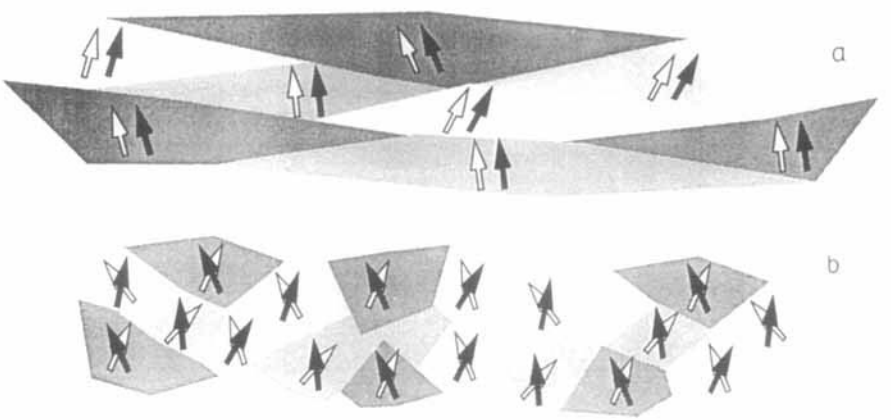

Fig. 5. Schematic diagram of a) the ripple and b) the patch pattern. Black arrows apply to the top layer, white ones to the bottom layer

3.3 Remanent domain patterns

Fig. 6 shows in more detail some characteristic patterns as they are observed in the field-free state in three areas of the first sample: an area with ferromagnetic coupling (Fig. 6a), an area with antiferromagnetic coupling (Fig. 6c), and a photograph from the intermediate zone (Fig. 6b).

The ferromagnetic patterns (Fig. 6a) are completely consistent with magnetization directions along the easy directions ⟨100⟩. At most four different grey shades can be made visible in the Kerr microscope near zero field. Regular 90°- and 180°-walls are oriented along the expected axes in order to avoid magnetic stray fields. Slightly charged zigzag walls which are occasionally observed (not shown) also agree with the well-known behaviour in ferromagnetic thin films. The assigment of magnetization direction arrows in the picture is consistent with all magnetic and magnetooptic experiments.

The antiferromagnetic pattern (Fig. 6c) develops out of the patch pattern (Fig. 4b) if the field is reduced to zero. The absence of any geometrical regularity indicates an antiparallel orientation of the magnetization in the two layers so that far-reaching stray fields cancel. As in the ferromagnetic case, four grey shades can appear in the field-free state in accordance with expectations, independent of the transparency of the films.

Strongly contrasting and at first sight confusing are the observations in the intermediate zone (Fig. 6b). Many of the walls follow strict geometrical rules in this pattern, but there are also peculiar rugged walls. A total of eight grey shades can be discovered with suitable microscope settings near zero field when playing around with the field. In nucleation

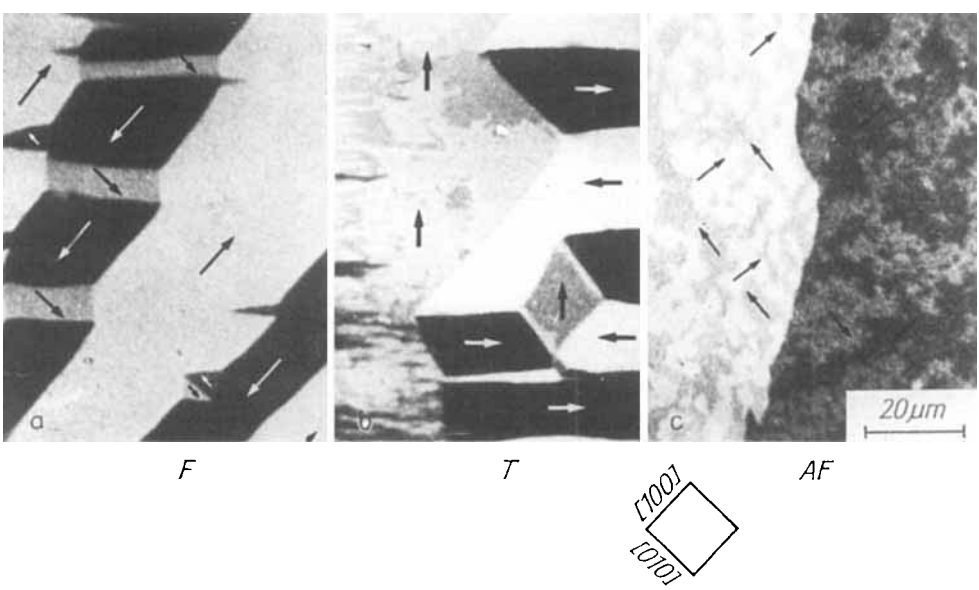

Fig. 6. High resolution domain images observed in three distinguishable zones of the (Fe 10 nm | Cr 0 to 3.7 nm | Fe 10 nm) sample: a) In the first ferromagnetically coupled zone, c) in the first antiferromagnetically coupled zone and b) in the first transition zone showing a domain pattern differing from both a) and c). The arrows in a) and c) indicate the magnetization of the top layer. In a) the bottom layer is magnetized parallel to the top layer, while in c) it is opposite to the top layer at each point. In b) the arrows indicate the presumed net magnetization of both layers. To the left of b) the characteristic "ripple" domains of the ferromagnetic region become visible

experiments we observe the patch domain pattern in this zone, so the basic interaction cannot be ferromagnetic. On the other hand, the regular geometrical domains at zero field exclude an antiferromagnetic nature of the coupling. The domains must carry a net magnetization at remanence, a conclusion which is corroborated by the relatively low switching field in this zone (Fig. 2). But this net magnetization cannot be oriented along the easy directions of the crystal. For example, we see domains with nearly rectangular corners in Fig. 6b with the domain walls on the sides of the corner oriented along ⟨100⟩. The magnetization in such a domain cannot be oriented along one of the walls because it would then meet the other wall head-on. The only consistent interpretation of the observed pattern assumes a net magnetization along the ⟨110⟩-axes as indicated in Fig. 6b by arrows! We assume that such a net magnetization is the result of the magnetization in the two layers along easy, but orthogonal ⟨100⟩-directions.

In this interpretation every phase magnetized along, say, the [110]-direction can be represented by two distinct subphases: one in which the top layer is magnetized along [100] and the bottom layer along [010], and another one with the magnetization in the two layers exchanged. If the Kerr effect sees mostly the top layer, but to a minor degree also the bottom layer, the two subphases should differ in their grey shade in the Kerr effect. The mentioned rugged walls demonstrate this contrast difference: they separate two domains with the same net magnetization so that the rules of flux closure do not command a particular orientation for these walls. Altogether eight different grey shades are expected to occur according to this model, in agreement with observations.

The nature of the observed phases and subphases in the transition zone can be confirmed and clarified by additional observations at perpendicular incidence. Under these conditions the Voigt effect and the magnetooptic gradient effect can be made visible using a $\lambda/10$-compensator. Fig. 7 shows a combination experiment [12] in which the same domain pattern was made visible at oblique incidence in the conventional Kerr effect (Fig. 7a) and at perpendicular incidence, displaying the Voigt and the gradient effect (Fig. 7b). The Voigt effect marks domains which are magnetized along different axes, but is independent of the sign of the magnetization vector. The gradient effect marks the domain boundaries in black or white depending on the magnetization difference vector between the two domains and on the orientation of the wall, both relative to the polarization axis of the light as explained in detail in [12] (Fig. 10 and (3)).

The interpretation shown in Fig. 7c is consistent with both observations in all details. The symbols indicate the net magnetization by the open arrows, the magnetization in the top layer by black arrows and in the bottom layer by hatched arrows. Look at the black arrows only to see the consistence with the Voigt contrast pattern and with the manifestations of the gradient effect in Fig. 7b. For a given top layer magnetization direction the bottom layer can, according to our model, assume two magnetization directions differing by roughly 180°. This makes no difference in the quadratic Voigt effect. In the case of the Voigt effect the contribution of the bottom layer therefore will weaken the observed contrast to some extent, but it will not modify the contrast depending on the magnetization direction of the bottom layer – as opposed to the case of the Kerr effect. The observation of only two grey shades in the Voigt effect is therefore consistent with the model. A similar argument applies to the gradient contrast at the domain boundaries. The contrast which can be derived from the rules using the magnetization in the top layer is the same for all possible configurations in the bottom layer as can be seen by a detailed analysis.

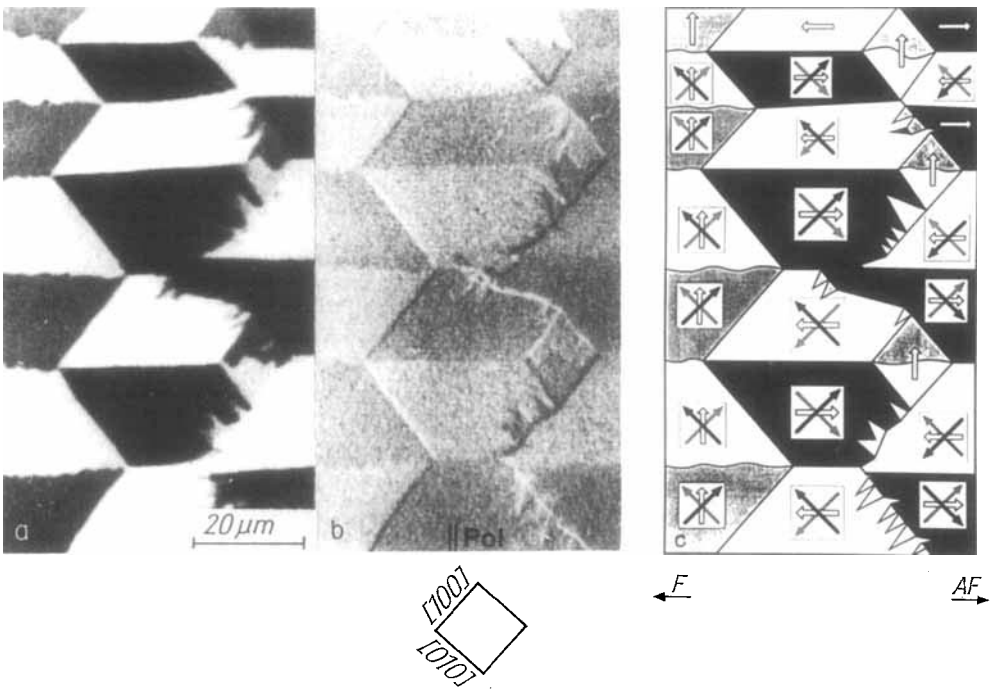

Fig. 7. A combination analysis of a domain pattern from the transition zone of the first sample, showing a) the Kerr effect, b) the Voigt and the gradient effect, and c) an interpretation consistent with all three aspects. The sample is close to the remanent state after saturation towards the top of the picture

In essence, the proposed interpretation of the observations in the intermediate zone postulates that the two layers prefer to be magnetized at 90° to each other rather than parallel or antiparallel. It was not possible to generate antiferromagnetically coupled domains in this zone for any field. The patch domain patterns observed after nucleation along the hard axis are consistent with a 90°-coupling as apparent from Fig. 5.

The pattern of Fig. 7 appears after a certain magnetization cycle of an applied field along the hard axis. Another pattern occurring frequently under similar circumstances is shown in Fig. 8. It can be understood along the same lines, using only canted states with a net magnetization along the ⟨110⟩ directions. No attempt is made to explain the detailed magnetization behaviour. It seems to be determined by slight asymmetries between the two layers in this sample, be it in the layer thickness or in coercivity. The continuously varying chromium interlayer thickness and the anisotropic sample shape also contribute to the behaviour of the domains as a function of an applied field. Instead of trying to understand all these details we will analyze in the following section the origin of the apparent preference for the orthogonal orientation of the magnetization in the two layers.

Detailed observations on another epitaxial sample basically confirmed the previous findings. This sample differed from the first one in two features: the iron layers were 20 nm thick each, and the slope of the chromium wedge was different, extending from zero to 2.05 nm over the 16 mm sample length. Fig. 9 shows the analysis of a domain pattern from the first transition zone. To understand these patterns we combined three magnetooptical methods in a single experiment: the longitudinal Kerr effect (Fig. 9a), the transverse Kerr

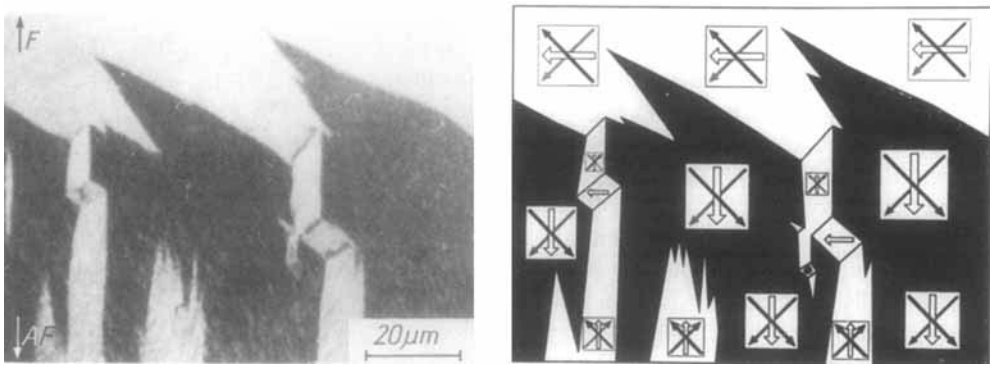

Fig. 8. Another type of pattern occurring in the intermediate zone under the same conditions as in Fig. 7 and analyzed in the same way. Again a net magnetization along the ⟨110⟩ axes and a preferred 90° orientation between the magnetization directions in the two layers has to be assumed. Partially charged zigzag walls replace some of the regular domain walls in a similar way often found in conventional single-layer films.

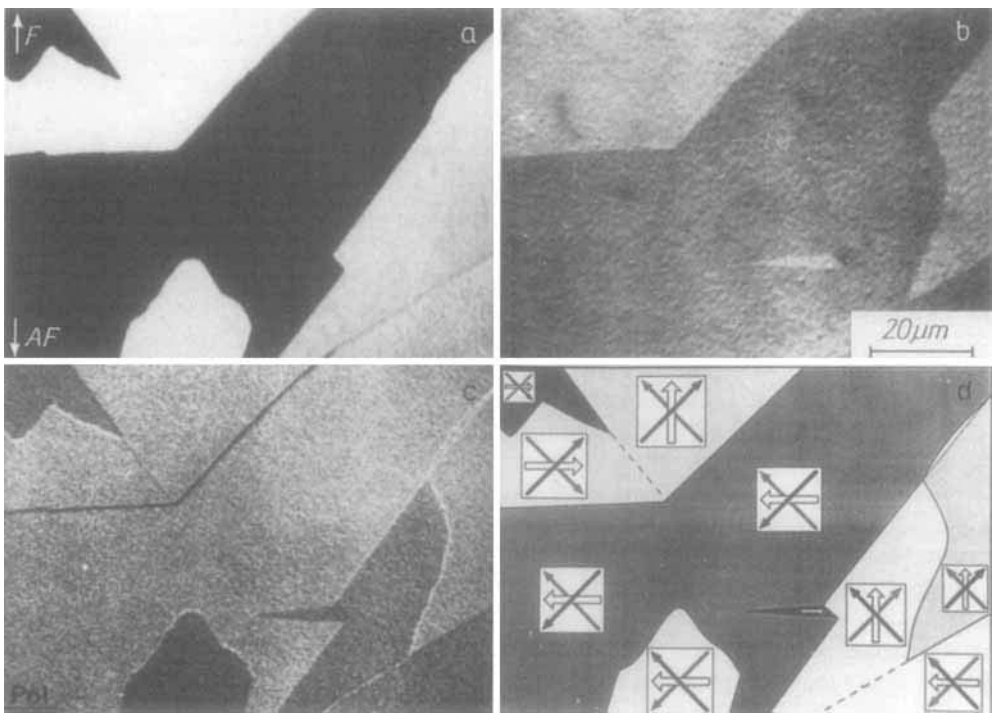

Fig. 9. An analysis of the first intermediate zone of (Fe 20 nm | Cr 0 to 2.05 nm | Fe 20 nm) sample. The four pictures show a) the longitudinal Kerr effect, b) the transverse Kerr effect, c) the Voigt and gradient contrast, and d) an interpretation of the observations as in Fig. 7. The grey shades and the black arrows in d) indicate the magnetization direction in the top layer as derived from (a to c). They are compatible with the overall flux closure pattern of the mean magnetization (open arrows)

effect (Fig. 9b) and the observation at perpendicular incidence offering the Voigt and the gradient effect (Fig. 9c). (Since no field could be applied in taking Fig. 9b, this picture was taken without image treatment directly from the video screen.)

The same interpretation as in Fig. 7 is possible in this case. The proposal of Fig. 9d is compatible with all observations and with the conventional domain rules. Note that some of the domains can barely be distinguished with the utilized techniques because they agree in their top layer magnetization, and because the information depth of the magnetooptical methods is smaller than the iron film thickness in the thicker sample. In the chosen example there can be no doubt about the placement of the hidden domains, particularly as the domain walls show up as a weak wall contrast (what we see is a quasi-wall induced by a Néel wall in the bottom layer for the purpose of charge compensation). There are more complicated images which may be a bit difficult to interpret, but the observation of domain wall motion can help considerably. One has to conclude that the canted coupling mode in the transition zone is confirmed in the thicker iron sample, but that thinner iron samples are better suited for fundamental studies of this kind because they allow to see through the top layer with magnetooptical methods to some extent.

The first transition zone of the same sample was also investigated at elevated temperatures. The width of the transition zone remained constant up to 200 °C and then shrunk reversibly by about one third up to 400 °C. This observation indicates that the transition zones represent a stable, equilibrium thermodynamic feature.

3.4 Easy axis magnetization curves

Examples of curves obtained with scanning Kerr measurements along one of the easy directions of the epitaxial iron films are shown in Fig. 10. The form of these curves was reproducible for different samples. In one sample the curves obtained for both easy axes were identical.

Fig. 10c and e demonstrate the existence of some phase with an average magnetization corresponding to one half of the saturation. (In these films the iron layers are only 3.0 nm thick so that the magnetooptic signal corresponds essentially to the mean value of both magnetic layers.) Taking into account the cubic crystal anisotropy such levels in the magnetization curves can only be explained by assuming that one of the films is magnetized along the field direction, while the other one is magnetized perpendicular to it. In the case of Fig. 10c the step in the magnetization curve extends from 100 to 170 Oe, while in Fig. 10e it ranges from 0 to 50 Oe. In both cases the intervals are much larger than the coercive force which is only around 5 Oe. This means that the phase which manifests itself in the steps in the magnetization curve must be stable and cannot represent some kind of metastable state.

The postulated transverse magnetization component could be observed magnetooptically in the two cases in which the intermediate steps were observed (Fig. 10c and e). The transverse component proved to be much smaller and highly hysteretic, however, probably due to the fact that both transverse magnetization components occurred in a mixed fashion.

4. Theoretical Analysis

4.1 Qualitative arguments

As the simplest approach we use the tools of phase theory, neglecting coercivity and all details of the actual domain pattern. If domains belonging to different phases (meaning

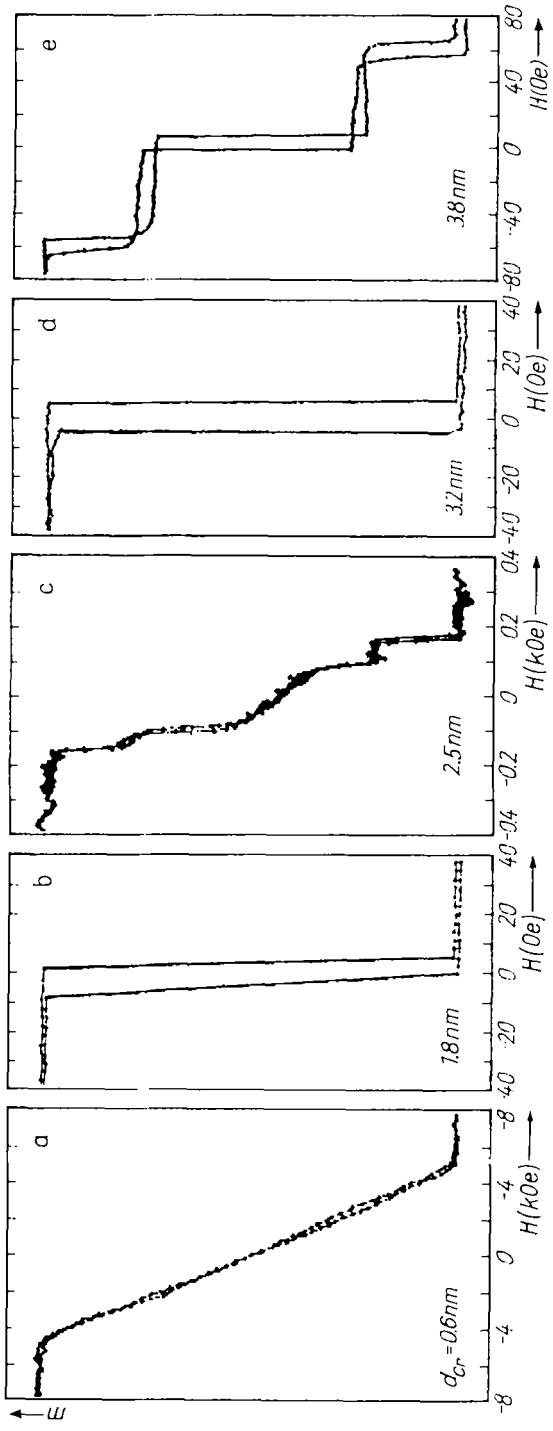

Fig. 10. Easy axis magnetization curves measured at different places of the Cr wedge. Note the different scales of the magnetic field for the different curves

that they are magnetized in different directions) coexist in thermodynamically equilibrium, their energies must be the same for a given value of the applied field (otherwise the domain walls separating them would move). We concluded from the experiments that in the transition zones domain phases with different net magnetization directions can coexist at zero field, where each phase consists of domains with essentially perpendicular magnetizations in the sublayers. Also in the magnetization curve measurements we observed phases with orthogonal magnetization arrangement in the two layers. Here we try to find out under which assumption this is possible.

In the first step we convince ourselves that this observation cannot be explained with a conventional ferromagnetic or antiferromagnetic coupling between the layers. The coupling between ferromagnetic layers is usually modelled after the Heisenberg interaction and assumed to be proportional to the scalar product $\boldsymbol{m}_1 \cdot \boldsymbol{m}_2$, where $\boldsymbol{m}_1$ is the unit vector parallel to the magnetization of the first layer and $\boldsymbol{m}_2$ the one of the second layer. Without an external field both magnetization directions will follow easy directions of the crystal, and if both layers are oriented in the same way, the coupling term will decide alone about the relative magnetization orientation of the two layers. But the cosine function in the Heisenberg term

has only two extrema, corresponding to the parallel and the antiparallel orientations. Depending on the sign of the coupling coefficient either one of these possibilities is preferred. The orthogonal orientation which would be allowed in terms of the cubic anisotropy is not allowed in zero field except when the coupling coefficient is exactly zero.

If the magnetic field is applied along an easy axis one can observe various kinds of spin flip transitions (a transition in which essentially the antiferromagnetic axis flips to an axis perpendicular to the applied field), but never long steps at half-saturation as in Fig. 10.

The situation changes when a biquadratic interaction term $(\boldsymbol{m}_1 \cdot \boldsymbol{m}_2)^2$ is admitted as first introduced in the analysis of spin structures in oxides [17]. A review of the occurrence and the consequences of such non-Heisenberg exchange effects can be found in [18]. The biquadratic coupling term [5]) alone has four extrema and may favour a 90° relative orientation. In order to understand better the consequences of this extension of the conventional concept of exchange interaction we calculate the magnetization curves in the approximation of phase theory. From this analysis we may deduce possible coexistent phases and compare them with observations.

4.2 Calculated magnetization curves

We assume uniform magnetization in both layers of thickness D_1 and D_2, characterized by the two angles θ and φ (Fig. 11).

The following contributions to the energy per unit area of the film system have to be considered:

Cubic crystal anisotropy,

$$E_K = 0.25K[D_1 \sin^2(2\theta) + D_2 \sin^2(2\varphi)]\,. \tag{1}$$

Coupling energy

$$\begin{aligned} E_c &= A_{12}[1 - \boldsymbol{m}_1 \cdot \boldsymbol{m}_2] + 2B_{12}[1 - (\boldsymbol{m}_1 \cdot \boldsymbol{m}_2)^2] \\ &= A_{12}[1 - \cos(\theta - \varphi)] + B_{12}[1 - \cos 2(\theta - \varphi)]\,. \end{aligned} \tag{2}$$

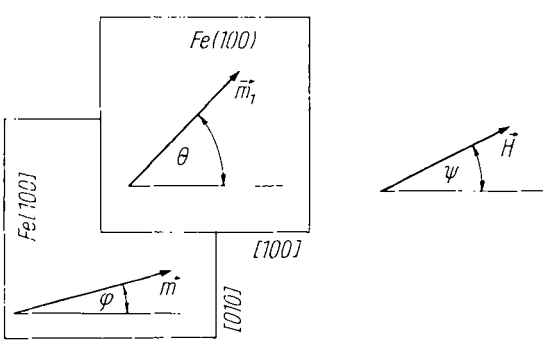

Fig. 11. The coordinates chosen for the analysis of the coupled layers

[5]) Under the assumption of in-plane magnetization the relation $1 - (\boldsymbol{m}_1 \cdot \boldsymbol{m}_2)^2 = [\boldsymbol{n} \cdot (\boldsymbol{m}_1 \times \boldsymbol{m}_2)]^2$ (where $\boldsymbol{n}$ is the surface normal) is valid. This indicates another possible interpretation of the biquadratic interaction in the sense of a second-order Dzyaloshinskii term instead of a second-order Heisenberg term. In this view the interaction would be related to spin orbit coupling rather than to exchange effects. Since in our samples the magnetization is always in-plane, our experiments cannot differentiate between the two alternatives. Both are clearly compatible with the symmetry of the problem.

External field energy (J_s is the saturation magnetization),

$$E_H = -HJ_s[D_1 \cos(\theta - \psi) + D_2 \cos(\theta - \psi)]. \tag{3}$$

Only the first-order cubic crystal anisotropy must be taken into account since the second-order term as well as first-order surface anisotropies do not contribute to the in-plane anisotropy of (100)-oriented samples. Considering the coupling energy alone there are three solutions as shown in Fig. 12a:

a) ferromagnetic coupling for $A_{12} > 0$ and $A_{12} > -4B_{12}$ with $\varphi = \theta$;
b) antiferromagnetic coupling for $A_{12} < 0$ and $A_{12} < 4B_{12}$ with $\varphi = \theta - \pi$;
c) a canted coupling for $B_{12} < 0$ and $|A_{12}| < -4B_{12}$
with $\varphi - \theta = \pm \arccos[-A_{12}/4B_{12}]$.

For multiple layers the canted coupling case could lead to a helical or an oscillating fan-like solution. Depending on the size of the first- and the second-order coupling constant a continuous variation of the coupling angle between 0° and 180° is predicted.

Including cubic anisotropy modifies the picture as shown in Fig. 12b. Now a preference for the coupling angles near 90° is found in the canted coupling regime. Analytically, the canted coupling is preferred in the case $D_1 = D_2 = D$ for

$$\frac{B_{12}}{DK} < 0; \qquad \left|\frac{A_{12}}{DK}\right| < \frac{-4B_{12}/DK}{1 + \sqrt{\dfrac{1}{1 - 4B_{12}/DK}}} \tag{4a}$$

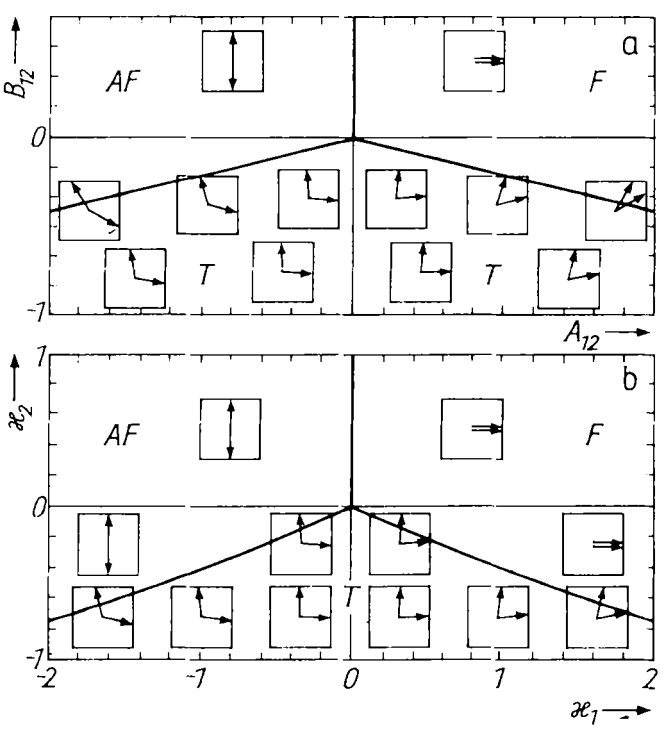

Fig. 12. Phase diagrams for the different magnetization arrangement in coupled films. a) With first- and second-order coupling only. b) Including cubic anisotropy for (100)-oriented films, assuming equal thicknesses $D_1 = D_2 = D$. The canting angle indicated at a few places in both phase diagrams is in a) only a function of the ratio $A_{12}:B_{12}$. In b) it converges under the influence of cubic anisotropy to 90° for small values of $\varkappa_1 = |A_{12}|/DK$ and $\varkappa_2 = |B_{12}|/DK$

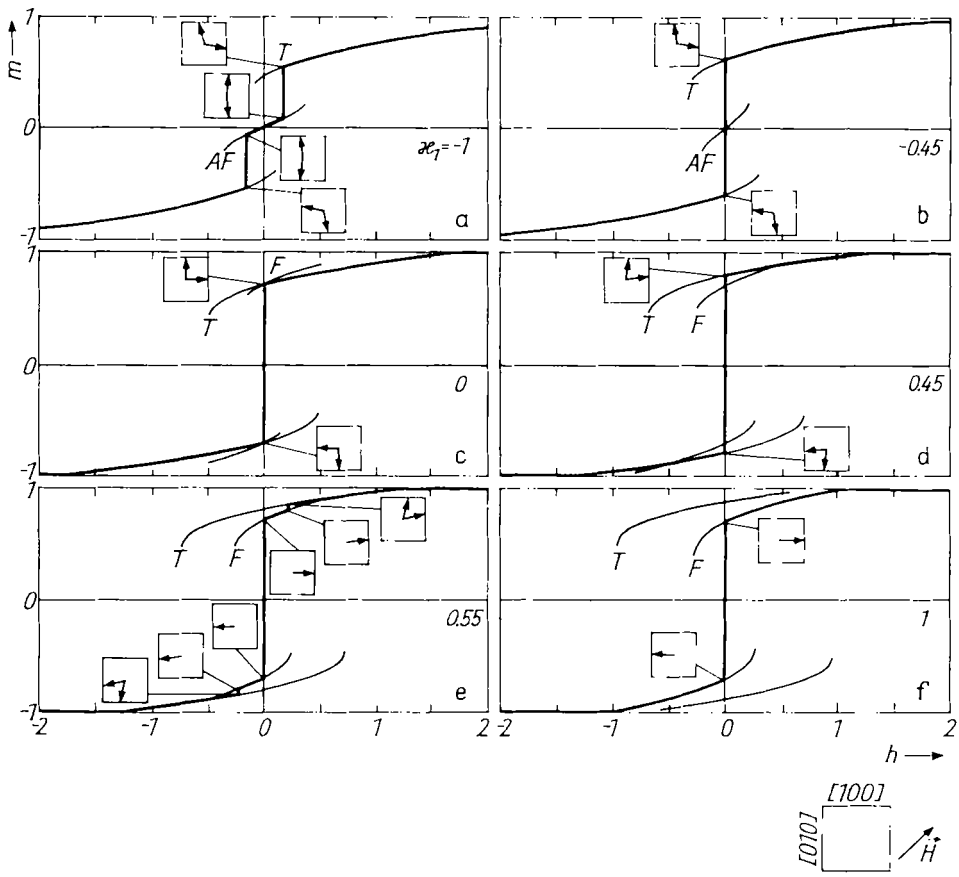

Fig. 13. Magnetization curves along the [110]-direction for a negative second-order coupling coefficient $\varkappa_2 = B_{12}/DK = -0.2$ and various values of the conventional first-order coupling constant indicated by the dimensionless parameter $\varkappa_1 = A_{12}/DK$. The fat anhysteretic magnetization curves are based on the absolute minimum in energy, while the thin lines indicate metastable states. a) is characteristic for the antiferromagnetic coupling, b) to d) are in the regime of canted coupling, while f) is in the ferromagnetic part of the phase diagram. The case e) represents another special transition between ferromagnetic and canted coupling. In b) to d) where canted states of opposite net magnetization can coexist at zero field, states with the net magnetization turned by 90° would also be possible. They were not included in the analysis

and for the canting angle we find

$$\varphi - \theta = \pm \arccos\left[\frac{A_{12}/DK}{1 - 4B_{12}/DK}\right]. \tag{4b}$$

The second-order coupling coefficient B_{12} must be negative to obtain a preferred canted coupling. For $|B_{12}|/|DK| \ll 1$ the limits of the canted state (4a) converge to $|A_{12}| < -2B_{12}$.

Including an applied field along the in-plane hard direction ($\varphi = 45°$) we calculated anhysteretic magnetization curves for $\varkappa_2 = B_{12}/DK < 0$ and various values of $\varkappa_1 = A_{12}/DK$ (Fig. 13). As expected, canted states with different net magnetization can only be simultaneously stable at zero field in the interval defined by (4a), that is, for negative $\varkappa_2$ and small

positive or negative values of $\varkappa_1$ (Fig. 13b to d). Canted states are also possible in the antiferromagnetic regime as in Fig. 13a. But here an applied field along a hard direction is necessary, and at this field only one canted phase with the net magnetization along the field is stable. The same type of magnetization curves as in Fig. 13a is found in the whole antiferromagnetic part of the phase diagram Fig. 12b, including the case $\varkappa_2 = 0$ and $\varkappa_1 < 0$. This means that the experiments cannot be understood with a first-order constant alone.

An unexpected secondary feature is predicted for $\varkappa_2 < 0$ and positive $\varkappa_1$-values between the regime (4a) of preferred canted coupling and the purely ferromagnetic regime beginning at $\varkappa_1 = -4\varkappa_2$. As shown in Fig. 13e, a canted configuration is expected in this case near nucleation, followed by a ferromagnetic arrangement at smaller fields and at remanence. An experimental verification of this peculiarity was found in a relatively narrow range adjacent to the previously discussed intermediate zone (Fig. 14). Here incipient patch domains were found to give way to a ripple-like pattern at lower fields. With the help of fast Fourier transform of the digitized image we succeeded in demonstrating this behaviour quantitatively. This analysis confirms the general conclusions, but it does not lead to any kind of additional insight.

We also calculated the magnetization curves for the field applied along the easy axis ($\psi = 0°$). The results are presented in Fig. 15. Steps in the magnetization curves are readily observed for $B_{12} < 0$ and for sufficiently small ratios $|A_{12}/B_{12}|$ (Fig. 15a to c). Admittedly, it is also possible to obtain similar steps in the magnetization curve without a second-order interaction, that is, for $B_{12} = 0$ under any of the following conditions: (i) an asymmetry in the magnetic moment of the two films, (ii) a deviation of the applied field from the easy direction, (iii) a difference of the orientation of the easy axes in the two films. In order to get the observed field interval of the canted phase, one would, however, have to postulate unrealistic values for these deviations: a 30% difference in the magnetic moment (which may actually be rather in the percent range), or a misalignment of the field of 7° (experimentally not more than 1°), or a misalignment of 6° between the easy axes (which is absent in the epitaxial films). All the mentioned deviations could, in addition, only generate magnetization curves as in Fig. 15a where the canted phase is stable at a finite applied

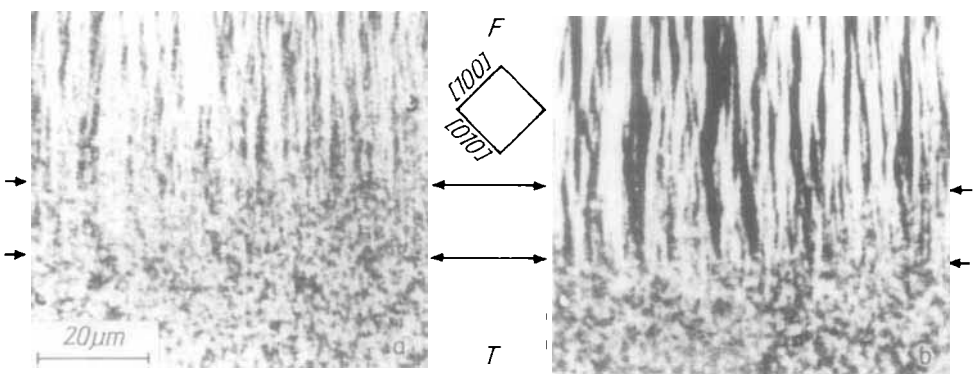

Fig. 14. Another peculiarity predicted by theory (Fig. 13e) and found in the ferromagnetic area close to the intermediate zone: a) In a narrow area indicated by lines the nucleation pattern is predominantly patch-like indicating an antiferromagnetic or canted coupling. b) At smaller fields a ripple pattern characteristic of ferromagnetic coupling takes over

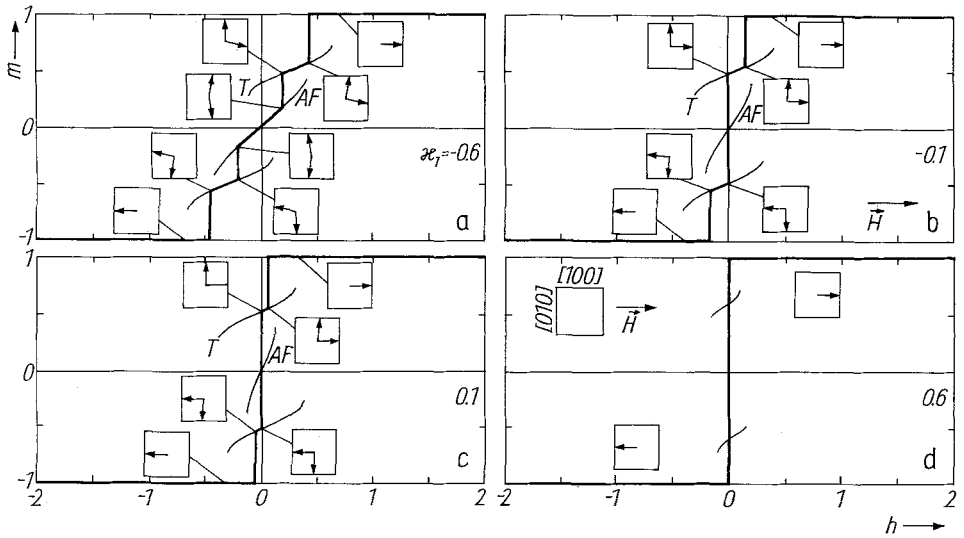

Fig. 15. Calculated easy-axis magnetization curves for $\varkappa_2 = -0.1$ and different values of $\varkappa_1$

field. The observation of stable canted states at zero field as calculated in Fig. 15b, c and measured in Fig. 10e proves directly the presence of a canted interaction in the same way as the observation of equilibrium canted domain states at zero field.

4.3 Estimating the size of the biquadratic coupling effect

The size of the second-order coupling effect can be derived from the width of the observed intermediate zones (Fig. 3) combined with the theoretical phase diagram (Fig. 12b). Eliminating the less well defined first sample from the argument, we obtain for the first transition zone an interval of about 0.025 nm thickness of the chromium interlayer around $d_{Cr} = 0.5$ nm. In the same way we get ≈ 0.06 nm for the second and ≈ 0.07 nm chromium layer thickness for the third transition layer.

Fig. 16 shows the measured values of the first-order coupling constant [2] of Fe–Cr–Fe multilayers. From the slope of the measured values of the coupling constant near the zero transitions we can derive the interval of the first-order coupling values for which the transition zone is observed. This interval is connected by (4a) with a value for the biquadratic coupling term. The results are marked in the figure by horizontal bars. Near the first transition the biquadratic term amounts to about 9% of the maximum antiferromagnetic coupling. At the site of the second transition the biquadratic coefficient appears to be reduced by about a factor of 15. The decay of the biquadratic coupling term with the chromium interlayer thickness follows roughly that of the first-order coupling term, but without any evidence of an oscillation.

In the derivation sketched above we assumed the biquadratic coupling coefficient to be approximately constant inside the transition zones. Assuming that B_{12} decays exponentially with the chromium thickness, a variation of B_{12} inside the first transition zone by about 10% would follow. Taking this variation into account would modify the conclusions only to a negligible degree.

From a fit of the curve in Fig. 10c it is possible to obtain a value for the ratio $|B_{12}/A_{12}| \approx 0.13$ for the centre of the second antiferromagnetic zone at around 2.5 nm Cr.

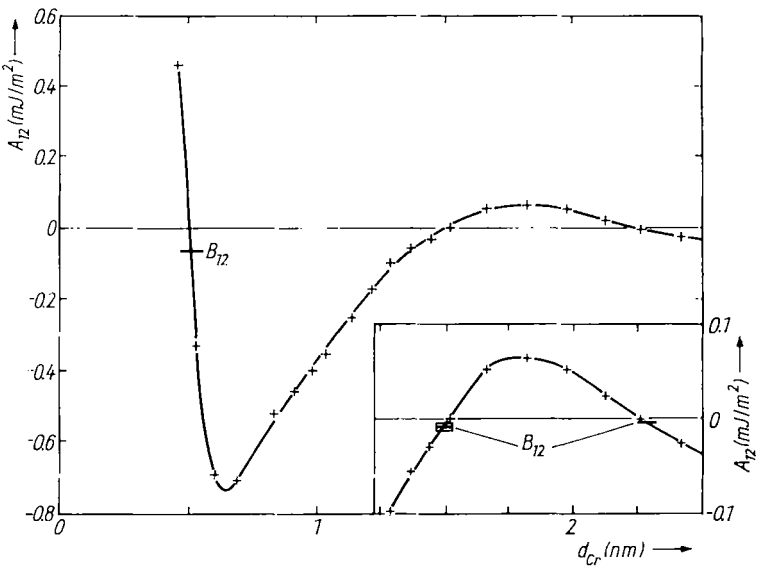

Fig. 16. The first-order coupling constant A_{12} as determined in [2] forms the basis for a quantitative estimate of the biquadratic coupling effect. Comparing the lengths of transition zones (Fig. 3) with the calculated interval (4a) and the measured curve we obtain the values for B_{12} near the three zero transitions of the first-order coupling

5. Further Observations

5.1 Thicker iron layers

We also investigated two samples with much larger iron thicknesses (30 and 40 nm). In these samples the areas of canted interaction appear to be much widened, interrupted in some cases only by narrow zones of ferro- or antiferromagnetic coupling. The observed interaction zones in the two samples are indicated in Fig. 17.

One conceivable difference compared to the thinner samples appears to be that the lattice mismatch between the silver buffer and the FeCr system which amounts to about 1% may be relaxed in the thick systems. Note that a planar strain would not generate any

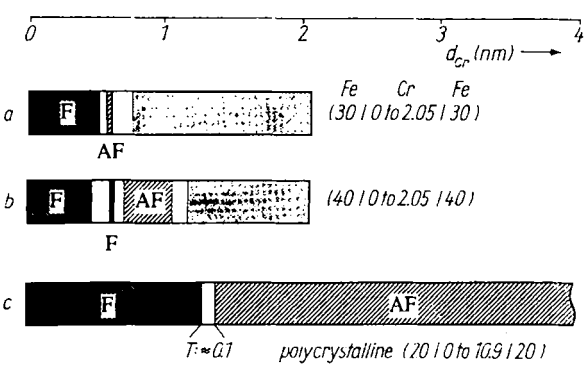

Fig. 17. a), b) The observed interaction zones in thick epitaxial iron samples and c) in a polycrystalline Fe–Cr–Fe system deposited by evaporation on glass. All thicknesses are shown in nm

in-plane anisotropy in the (100)-oriented films. One might speculate that the electronic properties of iron films strained by as much as 1% are sufficiently different from unstrained films to explain the observations.

5.2 Polycrystalline sample

The oscillating exchange effect was first discovered on polycrystalline samples [1]. Domain observation on polycrystalline iron samples is less rewarding due to an extremely strong ripple effect. Nevertheless, we discovered quite clear indications of an intermediate zone between ferromagnetic and antiferromagnetic coupling areas on a sample which was deposited on glass.

Fig. 18 shows an overview of the first transition and its neighbouring zones. The positions and lengths of these zones are indicated in Fig. 17. As in Fig. 4 we get a ripple pattern in the ferromagnetically coupled area and patches in the zone of antiferromagnetic exchange. In between, there is an area with mixed character which we identify with the transition zone. Higher resolution pictures from the three areas as shown in Fig. 19 confirm the distinct character of the intermediate zone.

6. Conclusions

Domain observation proved a very efficient tool for the identification of oscillating exchange in multilayer systems. It adds to the established macroscopic methods of optical, electron

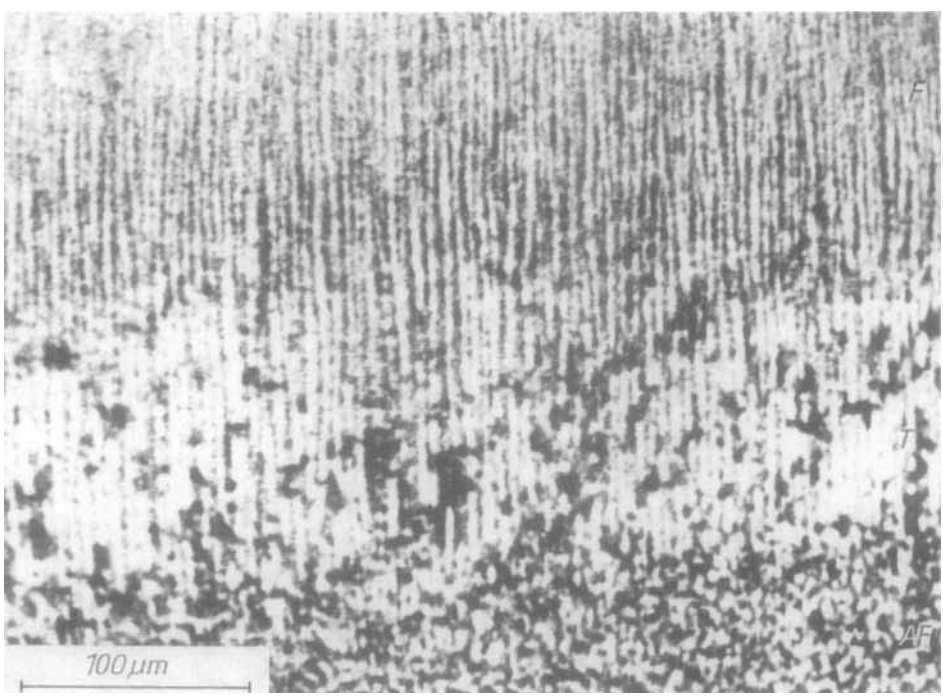

Fig. 18. A polycrystalline sample of 20 nm Fe layers separated by a chromium wedge shows a transition zone between ferromagnetic coupling (ripple pattern on the top) and antiferromagnetic coupling (patch domain pattern on bottom) in a nucleation experiment as in Fig. 4

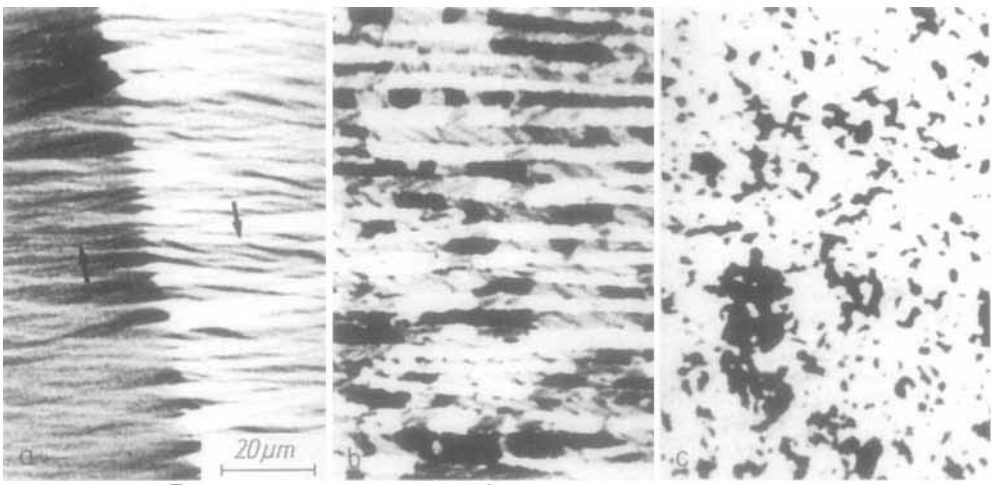

Fig. 19. High resolution pictures in a field free state from the same sample as in Fig. 18 confirm the distinct character of the domains in the intermediate zone (b). In a) (ferromagnetic coupling) a 180° domain wall enhances the ripple pattern in its neighbourhood. c) The patch domains generated at nucleation in the case of antiferromagnetic coupling coalesce to large patches in reduced fields. The peculiar perpendicular stripe pattern in the intermediate zone seems to be magnetized at $\pm 45°$ in the stripes as can be derived from Voigt effect pictures. Both the ripple and the stripes develop perpendicular to the previously applied field

spin, and spectroscopic measurements [1 to 3, 19] a microscopic method which allows to identify features which are present only on a micron scale. The detailed analysis of domain patterns as a function of the chromium interlayer thickness led to new insights on the nature of the coupling effect. The recently introduced magnetooptical effects available at perpendicular incidence helped greatly in this investigation.

We presented the first evidence for a biquadratic coupling effect on a macroscopic, domain level. The coupling leeds to an equilibrium canting angle near 90° between the magnetization directions in the ferromagnetic films. This property was found near the zero transitions of the oscillating first-order exchange interaction in the Fe–Cr–Fe system. Independently strong indications for a biquadratic coupling were also found in easy axis magnetization curves measured on antiferromagnetically coupled layers. A quantitative estimate puts the second-order coupling coefficient near the first intermediate zone (≈ 0.5 nm Cr) at about 9% of the maximum value of the first-order antiferromagnetic coupling constant which occurs at about 0.65 nm Cr in the Fe–Cr–Fe system according to spin wave measurements. The canted coupling was found in all investigated samples, although the relative widths of the different zones varied somewhat for unknown reasons. The phenomenon was found to be stable up to 400 °C, showing only a slight decrease in strength above 200 °C. A qualitatively deviating behaviour was found in samples with thicker iron films above 30 nm thickness.

Artificially modulated structures consisting of ferromagnetic layers with canted coupling represent a new magnetic material which may have unique properties, in particular in connection with magnetoresistive effects. Comparable substances with strongly canted spin structures [18] on the atomic level either have a low transition temperature, or are essentially antiferromagnetic, needing very high fields for saturation.

Acknowledgements

We thank Prof. W. Zinn for a hint about the previous use of the concept of biquadratic coupling and W. Habel for his assistance in photography. We also thank G. Traeger for the image Fourier analysis as well as H. Niedoba, H. Schewe, V. Florescu, and M. Donath for reading the manuscript and suggestions. Support by the CAMST program of European cooperation is gratefully acknowledged.

References

[1] P. GRÜNBERG, R. SCHREIBER, Y. PANG, U. WALZ, M. B. BRODSKY, and H. SOWERS, J. appl. Phys. **61**, 3750 (1987).
[2] S. S. P. PARKIN, N. MORE, and K. P. ROCHE, Phys. Rev. Letters **64**, 2304 (1990).
[3] P. GRÜNBERG, S. DEMOKRITOV, A. FUSS, M. VOHL, and J. A. WOLF, Conf. Magnetism and Magnetic Materials, San Diego 1990, J. appl. Phys., to be published (1991).
[4] H. HASEGAWA, Phys. Rev. B **42**, 2368 (1990).
[5] D. STOEFFLER, K. OUNADJELA, and F. GAUTIER, Proc. European Materials Research Society (E-MRS) Conf., Strassbourg 1990, Symp. C; J. Magnetism magnetic Mater., to be published 1991.
[6] Y. WANG, P. M. LEVY, and J. L. FRY, ibid.
[7] D. M. EDWARDS and J. MATHON, ibid.
[8] M. N. BAIBICH, J. M. BROTO, A. FERT, F. NGUYEN VAN DAU, F. PETROFF, P. ETIENNE, G. CREUZET, A. FRIEDERICH, and J. CHAZELAS, Phys. Rev. Letters **61**, 2472 (1988).
[9] G. BINASCH, P. GRÜNBERG, F. SAURENBACH, and W. ZINN, Phys. Rev. B. **39**, 4828 (1989).
[10] D. H. MOSCA, F. PETROFF, A. FERT, P. A. SCHROEDER, W. P. PRATT, JR., and R. LALOEE, J. Magnetism magnetic Mater. (1991), to be published.
[11] F. SCHMIDT, W. RAVE, and A. HUBERT, IEEE Trans. Magnetics **21**, 1596 (1985).
[12] R. SCHÄFER and A. HUBERT, phys. stat. sol. (a) **118**, 271 (1990).
[13] W. RAVE, R. SCHÄFER, and A. HUBERT, J. Magnetism magnetic Mater. **65**, 7 (1987).
[14] H. W. FULLER and M. E. HALE, J. appl. Phys. **31**, 238 (1960).
[15] K. J. HARTE, J. appl. Phys. **39**, 1503 (1968).
[16] H. HOFFMANN, IEEE Trans. Magnetics **4**, 32 (1968).
[17] E. A. HARRIS and J. OWEN, Phys. Rev. Letters **11**, 9 (1963).
D. S. RODBELL, I. S. JACOBS, J. OWEN, and E. A. HARRIS, Phys. Rev. Letters **11**, 10 (1963).
[18] E. L. NAGAEV, Soviet Phys. – Uspekhi **25** (1), 31 (1982).
[19] M. DONATH, D. SCHOLL, D. MAURI, and E. KAY, Phys. Rev. B (1991), to be published.

(Received March 21, 1991)